Efficient AoA-Based Rigid Body Localization via Single Base Station for Internet of Things Applications

BIAO ZHOU[1,2], **MINGMING ZHANG**[1,2], **YU-QIANG CHEN**[3], **NAIXUE XIONG**[4],
YUAN TIAN[5], **AND SABBIR AHMED**[1,2]
[1]School of Digital Media, Jiangnan University, Wuxi 214122, China
[2]School of IoT Engineering, Jiangnan University, Wuxi 214122, China
[3]Department of Computer Engineering, Dongguan Polytechnic, Dongguan 523808, China
[4]College of Intelligence and Computing, Tianjin University, Tianjin 300018, China
[5]School of Computer Engineering, Nanjing Institute of Technology, Nanjing 211167, China

Corresponding authors: Biao Zhou (zhoubiao@jiangnan.edu.cn) and Yu-Qiang Chen (chenyuqiang@126.com)

ABSTRACT For many data mining applications under the Internet of Things (IoT) environments, the attitude and the position of a rigid target are indispensable and hidden information to be dug. The term Rigid Body Localization (RBL) refers to simultaneously estimation of the position and the attitude of a rigid target. The RBL framework which adopts only one single base station (BS) is considered in this paper for IoT applications. Several wireless sensor nodes with known topology information are fixed on the surface of the rigid target. The single BS fuses the angle of arrival (AoA) measurements from the nodes with the topology information for the RBL purpose. In this paper, we propose a two-stage RBL method to efficiently fusing the aforementioned two pieces of information. Firstly, we built the maximum likelihood estimator (MLE) of the information fusion and adopted the modified Newton's iteration algorithm (mNIA) to determine the wireless node position; then we used the unit quaternion (UQ) algorithm for estimating the relative position and attitude with respect to the predetermined reference state, which completed the RBL task. Finally, we evaluated the proposed RBL performance in terms of the root mean squared error (RMSE), convergence success rate, as well as the computation costs. Simulation results showe that the proposed mNIA-based RBL algorithm can achieve a finer RBL performance with obviously higher speed and 100 percent success convergence rate, comparing with existing heuristic methods.

INDEX TERMS Internet of Things, heuristic algorithms, computational cost, rigid body localization, angle of arrival.

I. INTRODUCTION

The location information and the attitude information of the objects are of severe importance for many Internet of Things (IoT) applications [1], in cases where objects of interest are in rigid structure, i.e. rigid targets. The rigid object is the entity whose deformation can be neglected. The distance between any two points on the rigid body remains unchanged regard-

The associate editor coordinating the review of this manuscript and approving it for publication was Mu-Yen Chen.

less of the external force applied to it [2], [3]. In contrast with the conventional positioning schemes which only aim to find out the coordinates of the point source, the rigid body localization (RBL) can simultaneously estimate both the position and the attitude of a rigid target.

Rigid target localization has been playing an import role in the fields of smart sensing and the Internet of Things (IoT), including industries of entertainment, aerospace and manufacturing etc. The applications of RBL in the small-scale scenarios comprise virtual reality (VR) helmets, video

games and smart robots [4], simultaneous localization and mapping (SLAM) systems to name a few. The real-time three-dimensional (3-D) position and posture of VR helmets are essential information for VR systems to provide corresponding virtual images. In SLAM systems, the location and the orientation of the moving robots are needed to be fused with the environment sensing information in real time to build a map. The RBL is also applied to large-scale appliances such as vehicles, ships, aircraft, spaceships and buildings [5]. In space docking scenarios, the real-time and high precision information of the relative position and the attitude is crucial for posture adjustment during the docking process. In addition, the security departments have to collect the data from different types of sensors or even images from cameras and then perform the data mining on these information for monitoring the tilt and health of buildings, bridges etc. for the public safety.

The state-of-the-art reteaches regard the localization and the attitude estimation as two separate problems. Regardless of the attitude of the target object, plenty of researches on localization and tracking fields treat the target as a point source. The point source localization generally relies on the fusion of signal characteristic measurement in the smart sensing environments, including the satellites, Wi-Fi networks, and wireless sensor networks etc. The commonly adopted signal characteristic measurement includes the received signal strength (RSS), the time difference of arrival (TDoA), the time of arrival (ToA) and the angle of arrival (AoA) etc., [6]. The localization schemes based on RSS sensing own the upsides of low cost and easy implementation. However, the accuracy of the RSS-based localization schemes is as low as room-level because the RSS is susceptible to the varying environments. The positioning methods based on ToA and TDoA measurements can achieve high accuracy, but the synchronization problem is a practical challenge: ToA methods need the synchronization between the target and the base station (BS), while TDoA methods require the synchronization among the BSs, and a tiny clock shift can result in colossal positioning error due to the velocity of light.

On the other hand, the local attitude measurement is usually realized by the magnetometer, the gyroscope or other orientation-finding sensors [7], [8]. However, in a complex environment, the magnetometer fails to yield accurate readings and long term error accumulation makes the gyroscope obsolete. The orientation deciding approach based on the computer vision is another popular trend, in which several visible feature points should be marked on the target [9]–[11]; nevertheless this image-processing based technique is limited by the computational cost and the lighting condition.

II. RELATED WORKS AND CONTRIBUTIONS
A. PRIOR WORKS
Researches have acknowledged the necessity of simultaneously estimating the position and the attitude of rigid targets and tried several approaches to realize the RBL. One of the most popular methods is to utilize the global navigation

satellite systems (GNSSs), e.g. the GPS, the Compass system, etc. The GNSS is used for the RBL purpose as its derivative function. In the GNSS-based RBL schemes, several satellite receiving antennas should be equipped at known positions on the target to measure phases of arriving signal from at least 4 satellites. The phase differential technique is adopted for mitigating the propagation-related measuring error and for realizing the RBL purpose [9], [10]. However, the GNSS-based RBL method has to consider the problems of the period ambiguity in the phase measurement and the high hardware costs of the GNSS antennas. In addition, the GNSS-based RBL schemes are dedicated for large objects in outdoor environments and are not available anymore in Non-line of sight (NLOS) scenarios such as indoor and underwater areas.

The RBL schemes applied in IoT environments are widely studied, due to its advantages of high accuracy, low cost and easy carrying out [11]–[14]. Generally, smart sensing networks are setups where the terminals have the ability to capture signal characteristic measurements (including RSS, ToA, TDoA and AoA, etc.). In the RBL framework in IoT environments, several wireless sensor nodes are mounted on the rigid target. These nodes are relatively distributed in a known topology, which can be fully described by the Euclidean distances of all node pairs. While the positioning and the attitude estimation are being performed, the spatially distributed BSs measure the characteristics of signals from the wireless sensor nodes. After that, the RBL system fuses the sensed signal characteristic information with the known topology information to figure out the attitude information and the position information. Actually, different from GNSS-based RBL schemes which provide the absolute orientation and position information of the rigid target, the RBL framework in IoT environments is to provide the attitude and the position, relative to a predetermined *reference frame* of the target. Essentially, the current state of the rigid target to be estimated, also termed the *current frame*, is assumed to be obtained by the reference frame undergoing a rotation and a translation. In this way, the RBL is to estimate the translation vector and the rotation matrix. Actually, estimating the rotation matrix is a challenging problem, because it is a constrained 3-D Special Orthogonal $SO(3)$ group [11].

Abundant RBL works for IoT applications utilize the ranging technique, i.e., using the ToA or TDoA as the measurement to incorporate with the topology information for RBL purpose [10]–[15]. In the framework of RBL based on ranging techniques, ToA or TDoA between the wireless sensor nodes (mounted at a fixed position on the surface of the rigid target) and the base stations (BS) can be measured and converted into distances between wireless sensor nodes and BSs. To estimate the $SO(3)$ group and the 3D translation vector, Sundeep et.al first mitigated the nonlinearity of the RBL model by eliminating the quadratic unknown terms through an isometry decomposition of the projection matrix, and then proposed two types of least square estimators (LSEs) for deciding the rotation and translation information.

Moreover, the authors provided the constraint Cramér-Rao Bound (CCRB) for the ranging-based RBL framework as the rotation is belonging to $SO(3)$ group [11]. To further improve the computation efficiency, [12] used the traditional TDoA-based positioning method to find the coordinates of all wireless sensor nodes, and then adopted singular value decomposition (SVD) for obtaining a rough result, and then a refinement operation is performed with a non-iterative algorithm which obtained higher RBL accuracy and lower computational cost. Besides, they made use of the frequency difference of arrival (FDOA) measurements for estimating angular and translational velocities. Alternatively, authors in [13] utilized the semi-definite relaxation (SDR) algorithm to find an initial solution for the maximum likelihood estimator (MLE) of the TDOA-based RBL scheme to guarantee the estimation success under large noise conditions. The developed SDR-based method was proved to owning higher accuracy and lower computational cost, especially under high-level measurement noise. As the extension work of [13], the authors considered the additional function, i.e., realizing the velocities estimation, including the moving speed and rotational velocity under dynamic scenarios [14]. Moreover, in the recently published [15], Hao et.al paid attention on the RBL scenario under the problem of the BS position uncertainties and successfully applied the SDR algorithm for RBL purpose when the, moreover, the CCRB is provided as the quantitative analysis in terms of the BS location error.

However, the ranging-based RBL approaches have two tough issues to deal with when they are implemented in the realistic world. One issue is that the ranging techniques have a severe requirement (commonly nanosecond level) for the time synchronization due to the speed of electromagnetic wave [15]. To be specific, in the ToA-based ranging techniques, the synchronization between the source and the BS is needed, while TDoA-based ranging technique demands the synchronization among BSs. The other problem is that both the ToA and the TDoA method need four or more position-known BSs for 3-D localization in the IoT environments. This may be impractical in scenarios such as space docking where building spatially distributed BSs are not feasible, and in the complex environment where the line-of-sight link can not be guaranteed for all BS-node pairs. The research in [17] studied the relative positions and attitudes of multiple rigid targets by measuring the pairwise distance of wireless sensor nodes on multiple rigid targets with no need of the base stations (BS), however, this scheme is not efficient enough when objects are far apart from each other. When AoA is adopted as the measurement, the above two limitations can be eliminated.

In IoT environments, the AoA can be measured by the antenna array embedded in the BS. The antenna array consists of several antenna elements to sense the arriving signal phase, and numbers of readily algorithms have been studied for AoA estimation [18], such as the multiple signal classification (MUSIC) algorithm and matrix pencil (MP) algorithm etc. The 2-D AoA information measured in 3-D environment, including the azimuth and pitch angles, contains higher

information dimension than the ranging measurement (for example, for 2-D localization, the AoA technique for point source positioning needs two BSs while that of both ToA and TDoA are three), which make it possible realizing the RBL with a single BS. Besides, the AoA measuring cost is generally lower than that of the range measurement.

The AoA-based RBL framework was developed by Zhou et.al in [19] and [20]. In [19], they divided the RBL task into two stages. At the first stage, the 3-D coordinates of all the wireless sensor nodes in the current frame are obtained. They reduce the number of unknown arguments using AoA measurement and then find the unknown arguments using the particle swarm optimization (PSO) [21]–[23] topology information by setting the topology information as the cost function; then at the second stage, the rotation matrix and the translator vector are estimated by using SVD approach to compute the 3-D rigid body transformation that aligns the predetermined initial frame and the estimated current frame; the CCRB of the AoA-based RBL framework was derived as well. To enhance the RBL performance, a refinement process based on weighted least square (WLS) is performed at the first stage in the extension work [20]; in [20] they also replaced the PSO algorithm with participatory searching algorithm (PSA) for ensuring the global convergence success rate under the higher noise level. However, because of the high nonlinearity and the non-convexity of the AoA-based RBL model, the estimators based on heuristic search positioning algorithms, i.e., the PSA and the PSO algorithm, have a heavy calculation burden, which is not efficient enough in the practical application.

B. CONTRIBUTIONS
In this paper, we focus on improving the estimation success rate and the accuracy of the AoA-based RBL framework using a single BS for IoT applications, as well as reducing the computation cost. The proposed RBL estimator is divided into two stages.

At the first stage, we represent the known topology information and the AoA measurements as functions of 3D coordinates of the wireless sensor nodes, which form the current frame. Then, the current frame is estimated by the modified Newton iteration algorithm (mNIA) with a random initialization. It is well known that, the traditional Newton iteration algorithm (NIA), also termed the Gaussian-Newton method, has a high requirement for the initialization [24], [25]. In the proposed modified one, we set the iteration intervals for the parameters to be estimated using the known constraint of the parameters, i.e., the priori knowledge the application of the environment.

In the second stage, when the positions of wireless sensor nodes in the current frame are known, we can calculate the translation vector and the rotation matrix relative to the reference frame, by the unit quaternion (UQ) method. In the UQ method, instead of directly calculating the rotation matrix, we represent rotation employing a unit quaternion vector,
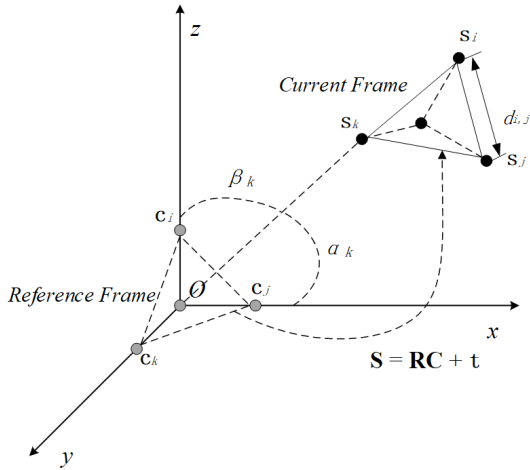
FIGURE 1. In AoA-based RBL framework, the current frame is arrived by undergoing a translation and a rotation.

which reduces the parameters to be estimated and avoid the challenging constraint problem.

The remainder of the paper is organized as follows. In Section III, the information collection for the AoA-based RBL framework via a single base station in the IoT is introduced and the corresponding MLE is built. Section IV discusses the process of determining 3D coordinates of the wireless sensor nodes mounted on the rigid object by the mNIA algorithm and solving transformation information of the object by the UQ method. In Section V, the performance of the proposed method is compared with that of existing estimators through simulations. Finally, a conclusion of the paper and our future work are given in Section VI.

For clarity, the notations used in this paper are shown as follows. $\|*\|$ means the Euclidian norm. Uppercase or lowercase bold letters are used to represent matrix and vectors, respectively. $\mathbf{X}^T$ is the transpose of $\mathbf{X}$, $\otimes$ is the notation of the Kronecker product, and $\mathbf{I}_n$ is the identity matrix of $n \times n$. $\mathbf{vec}(\mathbf{X})$ denotes the column vector which is obtained by stacking the columns of the matrix $\mathbf{X}$. $\mathbf{diag}(\mathbf{x})$ denotes the diagonal matrix whose main diagonal is the vector $\mathbf{x}$. $\mathbf{1}_{M \times N}(\mathbf{0}_{M \times N})$ denotes the $M \times N$ matrix of ones (zeros). $\mathbf{c}_\theta$ and $\mathbf{s}_\theta$ mean $\mathbf{cos}\,\theta$ and $\mathbf{sin}\,\theta$, respectively.

III. AOA-BASED RBL MODEL

In the AoA-based RBL framework implemented in IoT environments [29]–[39], one single BS and K wireless sensor nodes mounted on the rigid target form a network for deciding the location of the rigid target in 3-D space, as well as its gesture. The distribution of the K wireless sensor nodes on the target is known to a certain extent. As illustrated in Figure 1, the single BS is set as the origin O in the assumed coordinate system; a reference state of the target is set nearby the origin O and the current state of the target is to be estimated

A. REFERENCE FRAME DETERMINATION

Since our intent is to find the current state of the rigid target (comprising its position and its attitude) in the assumed
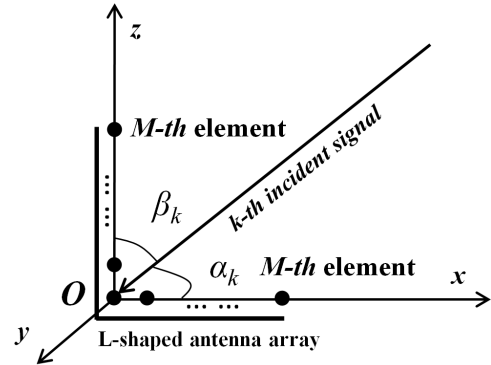

FIGURE 2. The structure of the LSAA at the single BS in the IoT environment for 3-D angle estimation.

coordinate system, a reference state should be determined in advance. The wireless sensor nodes under the reference state are termed the *reference frame*. In the reference frame, the coordinates of the kth wireless node are denoted as the vector $\mathbf{c}_k = [c_{k,x}, c_{k,y}, c_{k,z}]^T$, $k = 1, \ldots, k$, and the whole frame is presented by $\mathbf{C} = [\mathbf{c}_1, \ldots, \mathbf{c}_K] \in \mathbb{R}^{3 \times K}$.

In real applications, the immediate topology information of mounted nodes is the pairwise distances, by which $\mathbf{C}$ can be determined by the multidimensional scaling (MDS) technique [26], [27]. We collect the pairwise distance $d_{i,j}$ between i-th and j-th nodes and obtain a $K \times (K - 1)/2$ distance vector to present the relative topology information

$$\mathbf{d}^o = [d^o_{1,2}, \ldots, d^o_{i,j}, \ldots, d^o_{K-1,K}]^T, \quad i,j \in [1, \ldots, K], \ i < j. \tag{1}$$

We construct a zero-diagonal and symmetric squared distance matrix $\mathbf{D} \in \mathbb{R}^{K \times K}$, in which

$$\mathbf{D}(i,j) = \begin{cases} \left(d^o_{i,j}\right)^2, & \text{if } i \neq j \\ 0, & \text{if } i = j. \end{cases} \tag{2}$$

Then we define a centering matrix $E = I_M - \frac{1_{M \times M}}{M}$ and convert $\mathbf{D}$ into $\mathbf{B} = -\mathbf{E}\mathbf{D}\mathbf{E}^T/2 = \mathbf{E}\mathbf{C}^T\mathbf{C}\mathbf{E}^T$. Performing the eigenvalue decomposition (EVD) of $\mathbf{B}$ yields $\mathbf{B} = \mathbf{X}\,\text{diag}(\lambda_1, \lambda_2, \lambda_3)\mathbf{X}^T$, where $\lambda_1, \lambda_2, \lambda_3$ are the three largest non-zero eigenvalues in descending order, and their associated eigenvectors are collected in $\mathbf{X} \in \mathbb{R}^{K \times 3}$. Finally, the reference frame is acquired by

$$\mathbf{C} = \left[\mathbf{X}\text{diag}(\sqrt{\lambda_1}, \sqrt{\lambda_2}, \sqrt{\lambda_3})\right]^T. \tag{3}$$

Since $\mathbf{d}^o$ is measured in advance, the obtained reference frame $\mathbf{C}$ is regarded to be known precisely.

B. AOA ESTIMATION

For estimating 2-D AoA (the azimuth angle α and the pitching angle β), Figure 2 shows the structure of an L-shaped antenna array (LSAA) which is equipped at the single BS. $2M(M > K)$ antenna elements are uniformly arranged

along x and z axes with an interval of half-wavelength of the operating wireless signal.

When narrowband signals from K wireless sensors are impinging on the LSAA, all the antenna elements on x and z axes can sense the arriving phases, yielding the steering vector $\mathbf{g}_x$ and $\mathbf{g}_z$ [28], respectively; and their autocorrelation matrix is denoted as $\mathbf{G}_x = \mathrm{E}\{\mathbf{g}_x \mathbf{g}_x^H\}$ and $\mathbf{G}_z = \mathrm{E}\{\mathbf{g}_z \mathbf{g}_z^H\}$. If we adopt the MUSIC algorithm, the angles between kth impinging signal and two sides of LSAA, α_k^o and β_k^o can be estimated by searching the peaks from the pseudo-spectrum $P_{MUSIC}(\theta)$. For example, to estimate α_k^o, the pseudo-spectrum will be

$$\alpha_k^o = \arg\max P_{MUSIC}(\theta) = \frac{1}{a(\theta)^H G_w G_w^H a(\theta)}, \quad (4)$$

where $\mathbf{G}_w$ denotes the matrix in which the columns are the eigenvectors corresponding to the $M - K$ noise eigenvalues of the matrix $\mathbf{G}_x$, and these noise eigenvalues are typically much smaller than the remaining K eigenvalues. $a(\theta)$ presents the searching steering vector: $a(\theta) = [1, e^{-j\pi \cos\theta}, \ldots, e^{-j\pi(M-1)\cos\theta}]^T$. By the same analogy, β_k^o can also be estimated using the autocorrelation matrix $\mathbf{G}_z$.

C. RBL PROBLEM FORMULATION

The wireless node coordinates under the current state to be estimated are termed the *current frame*. Let the coordinates of k-th wireless node in the current frame be $\mathbf{s}_k = [s_{k,x}, s_{k,y}, s_{k,z}]^T$ and the coordinates of K wireless sensor nodes are collected in $\mathbf{S} = [\mathbf{s}_1, \mathbf{s}_2, \ldots, \mathbf{s}_K] \in \mathbb{R}^{3 \times K}$, $k = 1, \ldots, K$. According to the affine transformation, the current frame is transformed from the reference frame by rotation and translation as shown in Figure 1. Mathematically, $\mathbf{S}$ can be expressed as

$$\mathbf{S} = \mathbf{RC} + \mathbf{t} \otimes \mathbf{1}_{1 \times K}, \quad (5)$$

where $\mathbf{t} = [x, y, z]^T \in \mathbb{R}^{3 \times 1}$ and $\mathbf{R} \in \mathbb{R}^{3 \times 3}$ are the unknown translation vector and rotation matrix, respectively [27]. The rotation matrix $\mathbf{R}$ is an orthogonal matrix where the determinant is 1, i.e. $\mathbf{R}^T\mathbf{R} = \mathbf{R}\mathbf{R}^T = \mathbf{I}_3$. $\mathbf{t}$ and $\mathbf{R}$ respectively present the relative position and attitude with respect to predetermined $\mathbf{C}$, and finding $\mathbf{t}$ and $\mathbf{R}$ will complete the RBL task.

To find $\mathbf{t}$ and $\mathbf{R}$, $\mathbf{S}$ should be estimated first. For this purpose, two conditions are needed to be satisfied in the RBL estimation. The first one is the Euclidean distances between the node pairs on the rigid target. The known distance $d_{i,j}$ can be presented by the position of wireless sensor nodes in both frames that $d_{i,j}^o = \|\mathbf{c}_i - \mathbf{c}_j\|_2 = \|\mathbf{s}_i - \mathbf{s}_j\|_2$.

The second condition for RBL is the AoA measurements. The AoA is measured by the single BS, which are clearly presented in Section III-B. The ground truth of the angles between arriving signal from the nodes in the current frame and the x- and z-axes (see Figure 2) are denoted by are denoted by $\boldsymbol{\alpha}^o = [\alpha_1^o, \ldots, \alpha_K^o]^T$ and $\boldsymbol{\beta}^o = [\beta_1^o, \ldots, \beta_K^o]^T$, $k = 1, \ldots, k$.

In summary, the two conditions are functionally presented by the current frame to be estimated as follows:

$$\begin{cases} \alpha_k^o = \arccos \dfrac{s_{x,k}}{\sqrt{s_{x,k}^2 + s_{y,k}^2 + s_{z,k}^2}}, & k = 1, \ldots, K \\[2ex] \beta_k^o = \arccos \dfrac{s_{z,k}}{\sqrt{s_{x,k}^2 + s_{y,k}^2 + s_{z,k}^2}}, & k = 1, \ldots, K \\[2ex] d_{i,j}^o = \|\mathbf{s}_i - \mathbf{s}_j\|_2, & j > i \in [1, \ldots, K]. \end{cases}$$
$$(6)$$

Commonly, there is no root formula to solve the highly non-convex and nonlinear model above. Thus, we shall build the maximum likelihood estimator for the problem above.

We reshape the position of the wireless sensor nodes in the current frame to be estimated as a vector $\tilde{\mathbf{s}} = [\mathbf{s}_1^T, \ldots, \mathbf{s}_K^T]^T$ and reshape the known and measured noisy information as a vector $\boldsymbol{\gamma} = [\boldsymbol{\alpha}^T \boldsymbol{\beta}^T \mathbf{d}^T]$. In $\boldsymbol{\gamma}$,

$$\boldsymbol{\alpha} = [\alpha_1^o, \ldots, \alpha_K^o]^T + [\upsilon_{1,x}, \ldots, \upsilon_{K,x}]^T, \quad (7a)$$

$$\boldsymbol{\beta} = [\beta_1, \ldots, \beta_K]^T + [\upsilon_{1,z}, \ldots, \upsilon_{K,z}]^T, \quad (7b)$$

where $[\upsilon_{k,x}, \upsilon_{k,z}]^T \in \mathcal{N}(\mathbf{0}, [\sigma_{k,x}^2, \sigma_{k,z}^2]^T)$ are the additive Gaussian AoA measurement noise; and

$$\mathbf{d} = \mathbf{d}^o + \boldsymbol{n} \quad (8)$$

where $\boldsymbol{n} = [n_{1,2}, \ldots, n_{i,j}, \ldots, n_{K-1,K}]^T$ are the distance noise, and we assume it is in accord with the Gaussian distribution $n_{i,j} \in \mathcal{N}(0, \epsilon_{i,j}^2)$. Actually, the noise level of $[\boldsymbol{\alpha}^T \boldsymbol{\beta}^T]$ and $\mathbf{d}^T$ are different. $[\boldsymbol{\alpha}^T \boldsymbol{\beta}^T]$ are measured in real time with high-level noise, while $\mathbf{d}^T$ is predetermined with high reliability. Hence we decide $\epsilon_{i,j}^2$ to be an arbitrarily small and non-zero constant, say $\epsilon_{i,j} = 10^{-6}$ meter.

Then, the MLE is the minimizer of the cost function

$$\mathcal{J}_{ML} = (\boldsymbol{\gamma} - \bar{\boldsymbol{\gamma}}(\tilde{\mathbf{s}}))^T \mathbf{Q}^{-1} (\boldsymbol{\gamma} - \bar{\boldsymbol{\gamma}}(\tilde{\mathbf{s}})), \quad (9)$$

where $\bar{\boldsymbol{\gamma}}(\tilde{\mathbf{s}})$ is the reconstructed measurements according to Equation (6), and $\mathbf{Q}$ is the noise covariance matrix of $\boldsymbol{\gamma}$, which is defined as (10), as shown at the bottom of the next page.

The iteration-based method to solve the problem is presented in the next section.

IV. PROPOSED RBL ALGORITHMS

In the non-linear position estimating model presented in Equation (6), there are $3 \times K$ unknowns, and $K(K-1)/2 + 2K$ conditions which consist of $2K$ AoA measurements and $K(K-1)/2$ distances presenting the topology information. That is, the proposed model has a unique solution only when $K \geq 3$.

A. THE HEURISTIC ALGORITHMS

Obviously, it is impossible to find the analytical solution to minimize the cost function (9). The heuristic algorithms, including the PSO algorithm and the PSA method are very popular approaches for deciding the state of the object of interest in the data mining field and the implementations of heuristic algorithms are straight forward approaches.

Under similar RBL scenarios, the PSO algorithm and the PSA methods were implemented and described in detail in [18] and [19], respectively, thus we will not analyze implementations of heuristic algorithms here for the sake of concision. We only give the model for in the heuristic algorithms as follows

$$\min_{\tilde{\mathbf{s}}} \mathcal{J}_{ML}(\tilde{\mathbf{s}}|\boldsymbol{\alpha}, \boldsymbol{\beta}, \mathbf{d}), \quad \text{subject to } \tilde{\mathbf{s}} \in \textit{monitoring area}. \quad (11)$$

However, the drawbacks of the heuristic algorithm based approaches, that is, the high cost of computation and the low global convergence rate, limit its practical application, especially when the number of the arguments to be estimated is as many as $3 \times K$ since we intent to estimate $\mathbf{S}$.

B. THE MODIFIED NEWTON'S ITERATION METHOD

The Newton's iteration algorithm is one of the most efficient methods for finding the optimal solution of nonlinear models. The Newton's method is the process producing successively better approximations to the optimal value, and the advantages of Newton's method include the high speed of convergence and the high accuracy. However, the optimization process is susceptible to the initial value. Therefore, it is necessary to set an appropriate initial value, or to monitor the convergence process for guaranteeing the algorithm converges and ensuring its convergence speed.

Minimizing (9) by Newton's method is to linearize the nonlinear equations. The equation is expanded into the Taylor series at the initial value, and we can get an iterative relation by letting linear part of Taylor series to be zero if the derivative of the equation is not equal to zero. The method utilizes the derivative, and the direction of each iteration is the direction in which the value of the current point of the function decreases, which is detailed as follows.

In order to iteratively estimate the node positions expediently, we record the instant vectorized 3-D coordinates at t-th iteration as $\tilde{\mathbf{s}}_t$. Obviously, the angle measurements and the topology information of the current frame are determined by $\tilde{\mathbf{s}}_t$. Thus, we define an information vector as

$$\bar{\boldsymbol{\gamma}}(\tilde{\mathbf{s}}) = \begin{bmatrix} \bar{\boldsymbol{\alpha}}^T(\tilde{\mathbf{s}}_t) & \bar{\boldsymbol{\beta}}^T(\tilde{\mathbf{s}}) & \bar{\mathbf{d}}^T(\tilde{\mathbf{s}}) \end{bmatrix}^T, \quad (12)$$

where $\bar{\boldsymbol{\gamma}}(\tilde{\mathbf{s}}_t) \in \mathbb{R}^{(K(K-1)/2+2K)\times1}$ denotes the information vector yielded from $\tilde{\mathbf{s}}$ according to Equation (6). When $\tilde{\mathbf{s}}_t$ is the optimal solution $\tilde{\mathbf{s}}$, $\bar{\boldsymbol{\gamma}}(\tilde{\mathbf{s}}_t) = \boldsymbol{\gamma} = [\boldsymbol{\alpha}^T \boldsymbol{\beta}^T \mathbf{d}^T]^T$.

The beginning of the Newton iteration is performed by randomly setting the initial value of $\tilde{\mathbf{s}}$ to be estimated as $\tilde{\mathbf{s}}_0$. Afterwards, at t-th iteration of the Newton's method, we expand the cost function (9) at $\tilde{\mathbf{s}}_t$ by Taylor series and ignore the items whose order are higher than two, to linearize the

model and obtain

$$\bar{\boldsymbol{\gamma}}(\tilde{\mathbf{s}}_t) \approx \bar{\boldsymbol{\gamma}}(\tilde{\mathbf{s}}_t) + \mathbf{G} \cdot (\tilde{\mathbf{s}} - \tilde{\mathbf{s}}_t), \quad (13)$$

where $\mathbf{G} \in \mathbb{R}^{(K(K-1)/2+2K)\times 3K}$ is the Jacobian matrix of $\boldsymbol{\gamma}$, which is partially derived with respect to the coordinates of wireless sensor nodes in $\tilde{\mathbf{s}}$ and computed through

$$\mathbf{G} = \begin{bmatrix} \frac{\partial \boldsymbol{\alpha}^T}{\partial \tilde{\mathbf{s}}}|_{\tilde{\mathbf{s}}=\tilde{\mathbf{s}}_t} \\ \frac{\partial \boldsymbol{\beta}^T}{\partial \tilde{\mathbf{s}}}|_{\tilde{\mathbf{s}}=\tilde{\mathbf{s}}_t} \\ \frac{\partial \mathbf{d}^T}{\partial \tilde{\mathbf{s}}}|_{\tilde{\mathbf{s}}=\tilde{\mathbf{s}}_t} \end{bmatrix}, \quad (14)$$

where $\frac{\partial \boldsymbol{\alpha}^T}{\partial \tilde{\mathbf{s}}}$ and $\frac{\partial \boldsymbol{\beta}^T}{\partial \tilde{\mathbf{s}}}$ are the partial derivate of $\boldsymbol{\alpha}^T$ and $\boldsymbol{\beta}^T$ with respect to $\tilde{\mathbf{s}}$, and are matric in size of $K \times 3K$, $\frac{\partial \mathbf{d}^T}{\partial \tilde{\mathbf{s}}}$ is the partial derivate of $\mathbf{d}^T$ with respect to $\tilde{\mathbf{s}}$, and is a matrix of $\frac{(K-1)K}{2} \times 3K$. The expressions of $\frac{\partial \boldsymbol{\alpha}^T}{\partial \tilde{\mathbf{s}}}$, $\frac{\partial \boldsymbol{\beta}^T}{\partial \tilde{\mathbf{s}}}$ and $\frac{\partial \mathbf{d}^T}{\partial \tilde{\mathbf{s}}}$ are presented as follows respectively:

$$\frac{\partial \boldsymbol{\alpha}^T}{\partial \tilde{\mathbf{s}}} = \begin{bmatrix} \frac{\partial \alpha_1}{\partial x_1} & \frac{\partial \alpha_1}{\partial y_1} & \frac{\partial \alpha_1}{\partial z_1} & \cdots & \frac{\partial \alpha_1}{\partial x_K} & \frac{\partial \alpha_1}{\partial y_K} & \frac{\partial \alpha_1}{\partial z_K} \\ & \vdots & & & \vdots & & \vdots \\ \frac{\partial \alpha_K}{\partial x_1} & \frac{\partial \alpha_K}{\partial y_1} & \frac{\partial \alpha_K}{\partial z_1} & \cdots & \frac{\partial \alpha_K}{\partial x_K} & \frac{\partial \alpha_K}{\partial y_K} & \frac{\partial \alpha_K}{\partial z_K} \end{bmatrix}, \quad (15a)$$

$$\frac{\partial \boldsymbol{\beta}^T}{\partial \tilde{\mathbf{s}}} = \begin{bmatrix} \frac{\partial \beta_1}{\partial x_1} & \frac{\partial \beta_1}{\partial y_1} & \frac{\partial \beta_1}{\partial z_1} & \cdots & \frac{\partial \beta_1}{\partial x_K} & \frac{\partial \beta_1}{\partial y_K} & \frac{\partial \beta_1}{\partial z_K} \\ & \vdots & & & \vdots & & \vdots \\ \frac{\partial \beta_K}{\partial x_1} & \frac{\partial \beta_K}{\partial y_1} & \frac{\partial \beta_K}{\partial z_1} & \cdots & \frac{\partial \beta_K}{\partial x_K} & \frac{\partial \beta_K}{\partial y_K} & \frac{\partial \beta_K}{\partial z_K} \end{bmatrix} \quad (15b)$$

and (16), as shown at the bottom of the next page.

According to Equation (13), the gap between the instant information vector $\bar{\boldsymbol{\gamma}}(\tilde{\mathbf{s}}_t)$ and the actual information vector $\boldsymbol{\gamma}$ can be denoted by

$$\Delta = \boldsymbol{\gamma} - \bar{\boldsymbol{\gamma}}(\tilde{\mathbf{s}}_t) - \mathbf{G} \cdot (\tilde{\mathbf{s}} - \tilde{\mathbf{s}}_t). \quad (17)$$

In next iteration of the Newton's method, the update of $\mathbf{S}'_0$ is aiming to minimizing Δ. At instant update, the gap between $\tilde{\mathbf{s}}_t$ and the optimal solution can be obtained by

$$\boldsymbol{\delta} = \tilde{\mathbf{s}} - \tilde{\mathbf{s}}_t = \left(\mathbf{G}^T \mathbf{Q}^{-1} \mathbf{G}\right)^{-1} \mathbf{G}^T \mathbf{Q}^{-1} \left(\boldsymbol{\gamma} - \bar{\boldsymbol{\gamma}}(\tilde{\mathbf{s}}_t)\right). \quad (18)$$

where $\mathbf{Q}$ is the covariance matrix of the information vector which is a block diagonal matrix equaling to $\text{diag}(\mathbf{1}_{1\times 2K} \cdot \sigma, \mathbf{1}_{1\times \frac{K(K-1)}{2}} \cdot \varepsilon)^T$ in which σ and ε are the noise standards of AoA measurements and $\bar{\mathbf{d}}$, respectively. σ is larger than ε as the confidence of the topology is higher than that of the measurements. Thus in the next step, we can update the iterated value by replacing $\tilde{\mathbf{s}}_{t+1}$ with $\tilde{\mathbf{s}}_t + \boldsymbol{\delta}$

$$\mathbf{Q} = \begin{bmatrix} \text{diag}(\sigma_{1,x}^2, \ldots, \sigma_{K,x}^2, \sigma_{1,z}^2, \ldots, \sigma_{K,z}^2) & \mathbf{0}_{2K\times(K-1)K/2} \\ \mathbf{0}_{(K-1)K/2\times 2K} & \text{diag}(\epsilon_{1,2}^2, \ldots, \epsilon_{K-1,K}^2) \end{bmatrix} \quad (10)$$
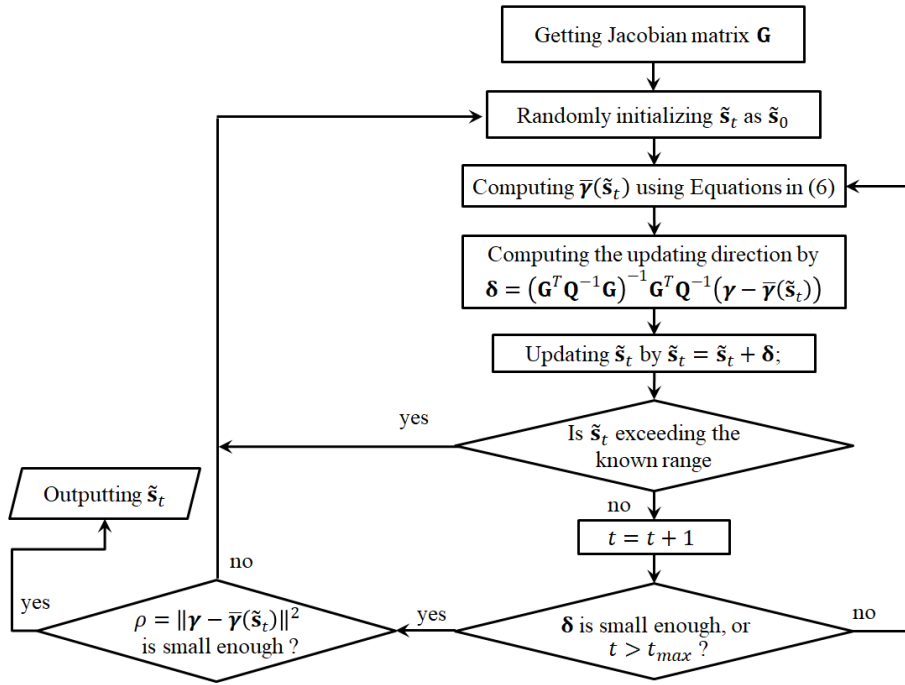
FIGURE 3. The modified Newton's iteration algorithm for getting the coordinates of the nodes in the current frame.

to mitigate the gap between the instant information vector and the actual information vector. Then, iteration is started again from Equation (13) using the updated $\tilde{\mathbf{s}}_{t+1}$. Above updating progress will not be stopped until $\|\boldsymbol{\delta}\|$ is sufficiently small and the optimization converges, or a maximum number of iterations has been reached. In the mNIA implementation, $\|\boldsymbol{\delta}\|$ is adaptively set in proportion to the noise level σ.

As we have discussed, the traditional Newton's method is easy to be unreliable when $\tilde{\mathbf{s}}_0$ is set far off from the ground truth. Thus, we make two modifications to the classic Newton's method. The first one is that the iteration monitoring. In a determined RBL scene, the ranges of the coordinates are known information, for example we can set the range according to the size of the RBL environment, or according to the communication distances from the single BS to the wireless sensors. When $\tilde{\mathbf{s}}_t$ is exceeding the predetermined ranges, we directly initialize $\tilde{\mathbf{s}}_0$ by randomly setting $\tilde{\mathbf{s}}_0$ as the

vector inside the predetermined ranges and begin the Newton iteration again.

The second modification is the criterion of the convergence quality. In traditional Newton's iteration, the convergence is accomplished when the updating step $\boldsymbol{\delta}$ is small enough. Here, we conduct an additional convergence quality checking process. When the updating progress is stopped (when $\boldsymbol{\delta}$ is small enough or the maximum iteration number is reached), we will compute the matching degree of the information vector yielded from the final $\tilde{\mathbf{s}}_0$ and the actual the information vector, and denote it as $\rho = \left\| \boldsymbol{\gamma} - \bar{\boldsymbol{\gamma}}\left(\tilde{\mathbf{s}}_t\right) \right\|^2$. If ρ is larger than the predetermined threshold, we directly initialize $\tilde{\mathbf{s}}_0$ by randomly setting $\tilde{\mathbf{s}}_0$ as the vector inside the predetermined ranges and begin the Newton iteration again.

Forthrightly, we add two judgments in the modified Newton's iteration algorithm to fuse the known positioning range information and the information vector which ensures the convergence success, as shown in Figure 3. Through the

$$
\frac{\partial \mathbf{d}^T}{\partial \tilde{\mathbf{s}}} = \begin{bmatrix} \frac{\partial d_{1,2}}{\partial x_1} & \frac{\partial d_{1,2}}{\partial y_1} & \frac{\partial d_{1,2}}{\partial z_1} & \cdots & \frac{\partial d_{1,2}}{\partial x_K} & \frac{\partial d_{1,2}}{\partial y_K} & \frac{\partial d_{1,2}}{\partial z_K} \\ & \vdots & & \vdots & & \vdots & \\ \frac{\partial d_{i,j}}{\partial x_1} & \frac{\partial d_{i,j}}{\partial y_1} & \frac{\partial d_{i,j}}{\partial z_1} & \cdots & \frac{\partial d_{i,j}}{\partial x_K} & \frac{\partial d_{i,j}}{\partial y_K} & \frac{\partial d_{i,j}}{\partial z_K} \\ & \vdots & & \vdots & & \vdots & \\ \frac{\partial d_{K-1,K}}{\partial x_1} & \frac{\partial d_{K-1,K}}{\partial y_1} & \frac{\partial d_{K-1,K}}{\partial z_1} & \cdots & \frac{\partial d_{K-1,K}}{\partial x_K} & \frac{\partial d_{K-1,K}}{\partial y_K} & \frac{\partial d_{K-1,K}}{\partial z_K} \end{bmatrix} \tag{16}
$$

modified Newton's iteration algorithm, the current frame is estimated. Until now, we get the reference frame $\mathbf{C}$ and the current frame $\mathbf{S}$.

C. DETERMINATION OF R AND t BY THE UNIT QUATERNION ALGORITHM

After getting the optimal $\mathbf{S}$ through heuristic methods or Newton's method, the rotation matrix $\mathbf{R}$ and the translation vector $\mathbf{t}$ of the rigid body, with respect to the reference frame, will be determined.

In the transformation Formula (5), $\mathbf{S}$ and $\mathbf{C}$ are known. In this section, the translation vector $\mathbf{t}$ and the rotation matrix $\mathbf{R}$ shall be computed by the unit quaternion (UQ) method. The UQ method uses a 3×1 vector $\boldsymbol{\psi} = [l, m, n]^T$ to represent the rotation axis and an angular component θ to represent the angle of rotation around this axis [29]. Using $\boldsymbol{\psi}$ and θ, a UQ is defined as

$$
\begin{aligned}
\mathbf{q} &= [q_0, \quad q_1, \quad q_2, \quad q_3]^T \\
&= [c_{\theta/2}, \quad ls_{\theta/2}, \quad ms_{\theta/2}, \quad ns_{\theta/2}]^T,
\end{aligned} \quad (19)
$$

where the 3-D vector (l, m, n) meets $l^2 + m^2 + n^2 = 1$ is the rotation axis. Moreover, the rotation matrix $\mathbf{R}$ can be derived from the Rodrigues formula (20), as shown at the bottom of this page, where $\mathbf{U} = \begin{bmatrix} 0 & -n & m \\ n & 0 & -l \\ -m & l & 0 \end{bmatrix}$ is the cross product matrix of the rotary axis (l, m, n), substituting $\mathbf{q}$ to Equation (20) and we can get rotation matrix [30], (21), as shown at the bottom of this page,

Then $\mathbf{q}$ is the solution which minimizes the following least square error:

$$
\begin{aligned}
\varepsilon^2 &= \sum_{k=1}^{K} \|s_k - \mathbf{R}c_k + \mathbf{t}\|^2 = \sum_{k=1}^{K} \|s_k' - \mathbf{R}c_k'\|^2 \\
&= \sum_{k=1}^{K} (s_k'^T s_k' + c_k'^T c_k' - 2s_k'^T \mathbf{R}c_k'),
\end{aligned} \quad (22)
$$

where $s_k' = s_k - \bar{s}$, $c_k' = c_k - \bar{c}$, and $\bar{s}$, $\bar{c}$ are means of s_k and c_k respectively. The least square error can be rewritten as $\varepsilon^2 = \mathbf{q}^T \mathbf{P} \mathbf{q}$ according to the attributes of the quaternion, and $\mathbf{P}$ is a matrix of 4×4 denoted by (23), as shown at

the bottom of this page, where $H_{ab} = \sum_{k=1}^{K} c_{k,a}' s_{k,b}'$, $a, b \in (x, y, z)$, the UQ $\mathbf{q}$ is the eigenvector corresponding to the largest eigenvalue of matrix $\mathbf{P}$. Thus $\boldsymbol{\psi}$ and θ are calculated by Equation (18). Finally, the rotation matrix $\mathbf{R}$ can be obtained from (20) with the known $\boldsymbol{\psi}$ and θ, and the translation vector $\mathbf{t}$ can be obtained by substitute $\mathbf{R}$ into Equation (5).

V. PERFORMANCE EVALUATION

In this section, we shall evaluate the performance of the two-stage AoA-based RBL scheme proposed in this paper. Predefined parameters are set including the distances between node pairs which are utilized to obtain the reference frame, as well as the rotation matrix and the translation vector by which the current frame is obtained from the reference frame. The pilot runs are carried out in simulation environment individually for each of four methods, which include the traditional Newton iteration algorithm and the proposed modified Newton iteration algorithm with the information fusing mentioned in Section 3.3, as well as the two heuristic methods, i.e., the PSO method and the PSA method. We focus on the efficiency of the AoA-based RBL model and the results are carefully observed and compared with each other to find out the method with high convergence speed and high success rate and outstanding accuracy.

A. SIMULATION ENVIRONMENT

In the simulated AoA-based RBL scenario with a single BS, we consider $K = 4$ wireless sensor nodes mounted on rigid objects with different sizes, and the distances between node pairs are precisely measured to be

$$
\begin{aligned}
\mathbf{d}_o &= [d_{1,2}, \quad d_{1,3}, \quad d_{1,4}, \quad d_{2,3}, \quad d_{2,4}, \quad d_{3,4}] \\
&= [1, \quad 1, \quad 1, \quad \sqrt{2}, \quad \sqrt{2}, \quad \sqrt{2}] \times D,
\end{aligned} \quad (24)
$$

where D is the size of the targets. According to the distance information between wireless sensor pairs, the reference frame is determined by the MDS algorithm as

$$
\mathbf{C} = \begin{bmatrix} 0 & 1 & 0 & 0 \\ 0 & 0 & 1 & 0 \\ 0 & 0 & 0 & 1 \end{bmatrix} \times D, \quad (25)
$$

$$
\mathbf{R} = \mathbf{I}_3 + 2\mathbf{U} \cdot s_{\theta/2} \cdot c_{\theta/2} + 2s_{\theta/2}^2 \cdot \mathbf{U}^T \mathbf{U}
$$

$$
= \begin{bmatrix}
1 - 2(m^2 + n^2)s_{\theta/2}^2 & 2lms_{\theta/2}^2 - 2ns_{\theta/2}c_{\theta/2} & 2lns_{\theta/2}^2 + 2ms_{\theta/2}c_{\theta/2} \\
2lms_{\theta/2}^2 + 2ns_{\theta/2}c_{\theta/2} & 1 - 2(l^2 + n^2)s_{\theta/2}^2 & 2mns_{\theta/2}^2 - 2ls_{\theta/2}c_{\theta/2} \\
2lns_{\theta/2}^2 - 2ms_{\theta/2}c_{\theta/2} & 2mns_{\theta/2}^2 + 2ls_{\theta/2}c_{\theta/2} & 1 - 2(l^2 + m^2)s_{\theta/2}^2
\end{bmatrix} \quad (20)
$$

$$
\mathbf{R} = \begin{bmatrix}
q_0^2 + q_1^2 - q_2^2 - q_3^2 & 2(q_1q_2 - q_0q_3) & 2(q_0q_2 + q_1q_3) \\
2(q_0q_3 + q_1q_2) & q_0^2 - q_1^2 + q_2^2 - q_3^2 & 2(q_2q_3 - q_0q_1) \\
2(q_1q_3 - q_0q_2) & 2(q_0q_1 + q_2q_3) & q_0^2 - q_1^2 - q_2^2 + q_3^2
\end{bmatrix} \quad (21)
$$

$$
\mathbf{P} = \begin{bmatrix}
H_{xx} + H_{yy} + H_{zz} & H_{yz} - H_{zy} & H_{zx} - H_{xz} & H_{xy} - H_{yx} \\
H_{yz} - H_{zy} & H_{xx} - H_{yy} - H_{zz} & H_{xy} + H_{yx} & H_{zx} + H_{xz} \\
H_{zx} - H_{xz} & H_{xy} + H_{yx} & H_{yy} - H_{xx} - H_{zz} & H_{yz} + H_{zy} \\
H_{xy} - H_{yx} & H_{zx} + H_{xz} & H_{yz} + H_{zy} & H_{zz} - H_{xx} - H_{yy}
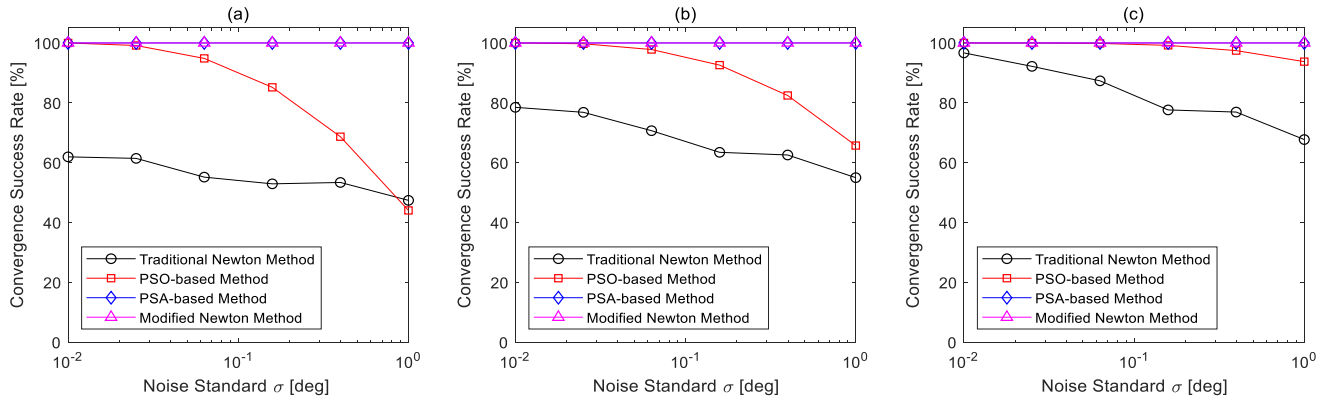\end{bmatrix} \quad (23)
$$

FIGURE 4. The convergence success rate of the four methods under different vs. noise standards and rigid target sizes (a) *D* = 1 meter: (b) *D* = 2 meters, (c) *D* = 3 meters.

which means the wireless sensor nodes are distributed as a four-sided pyramid with a bottom of equilateral triangle and three sides of isosceles right triangles in the reference frame. The ground truth of the current frame is obtained from the reference frame by rotating $[\,30 \quad -50 \quad 80\,]^T$ degrees along x, y, z axes, respectively and then by a translating vector $\mathbf{t} = [6\,5\,2]^T$ meters, meaning that the rigid target is 8 meters far away from the reference frame.

Signal arriving angles from the wireless sensors to the single BS (fixed at the origin) is measured with noise. We assume that the AoA measurement noises are independent and identically distributed as white Gaussian noise with the same standard σ, i.e. $\sigma_{k,x}^2 = \sigma_{k,z}^2 = \sigma^2$.

Under above parameters assumption, the simulation is carried out with MATLAB on a 3.5 GHz personal computer.. The four methods are simulated for finding the optimal current frame and 18 cases are considered for each method (6 noise levels × 3 different rigid target sizes).

B. PERFORMANCE EVALUATION

The simulations are conducted over $N = 1000$ independent Monte Carlo runs for each of the four estimation approaches, and their performances are evaluated in terms of convergence success rate (CSR), computing cost of the simulation experiment, and the root mean squared error (RMSE) of the estimates.

To investigate the effectiveness of the mNIA method on the convergence success rate, we set different and random initial value to **S** at the beginning of each iteration. Besides, the random initial value $\mathbf{S}_0$ are all generated within the known range (Unit: meter), which is assumed as $0 < s_{x,k} < 10$, $0 < s_{y,k} < 10$, and $0 < s_{z,k} < 5$, $k = 1, \ldots, K$. The comparison among the four methods is shown in Figure 4.

Results in Figure 4 show that the larger size of the rigid target can enhance the CSR, for the PSO method and the traditional Newton method. For the traditional Newton method, the improvement is slight, because this method relies heavily on the initial value of the iteration process. It is observed that the modified Newton method and the PSA method can

TABLE 1. The computation time (in seconds) of NIA, mNIA, PSA and PSO methods when *D* = 2 meters.

σ [deg]	10^{-2}	10^{-1}	10^{0}
PSO	7.94 s	7.38 s	10.45 s
PSA	5.36 s	5.91 s	8.97 s
NIA	1.1×10^{-3}s	1.5×10^{-3}s	1.8×10^{-3} s
mNIA	1.5×10^{-3}s	3.2×10^{-3}s	7.7×10^{-3} s

guarantee 100 percent CSR in all cases, which verifies the effectiveness of the modified Newton method. Actually, the two additional judgement links in Figure 3 ensure the CSR. However, comparing with the traditional Newton method, these two links increase the computational cost.

In Table 1, the average time cost per Monte Carlo runs of the four methods under different cases are listed. It is apparent that Newton's methods outperform the heuristic methods, since the each convergence of the heuristic methods is as high as several seconds while that of Newton's methods is recorded in milliseconds. Although the success rate of the PSA method and the proposed mNIA method all reach 100%, the computational expenditure of the former is much higher than the later one. In addition, as the noise increases, the gap between the NIA method and the mNIA method grows larger. The reason behind is that when an improper initial value causes convergence failure, a new random initial value is given for another Newton iteration for searching the optimal solution, until the instant information vector matches the actual information vector; and the higher noise level increases the afresh searching possibility, thereby more convergence time is required; nevertheless, its computational efficiency is still much higher than the existing heuristic methods.

Finally, we evaluate the accuracy of the four methods in terms of the RMSE of the estimates of **R** and **t** which are computed by [10]

$$\mathrm{RMSE}\,(\mathbf{R}) = \sqrt{\frac{1}{N}\sum\nolimits_{n=1}^{N}\left\|\mathbf{R} - \hat{\mathbf{R}}_n\right\|}, \qquad (26)$$

$$\mathrm{RMSE}\,(\mathbf{t}) = \sqrt{\frac{1}{N}\sum\nolimits_{n=1}^{N}\left\|\mathbf{t} - \hat{\mathbf{t}}_n\right\|}, \qquad (27)$$

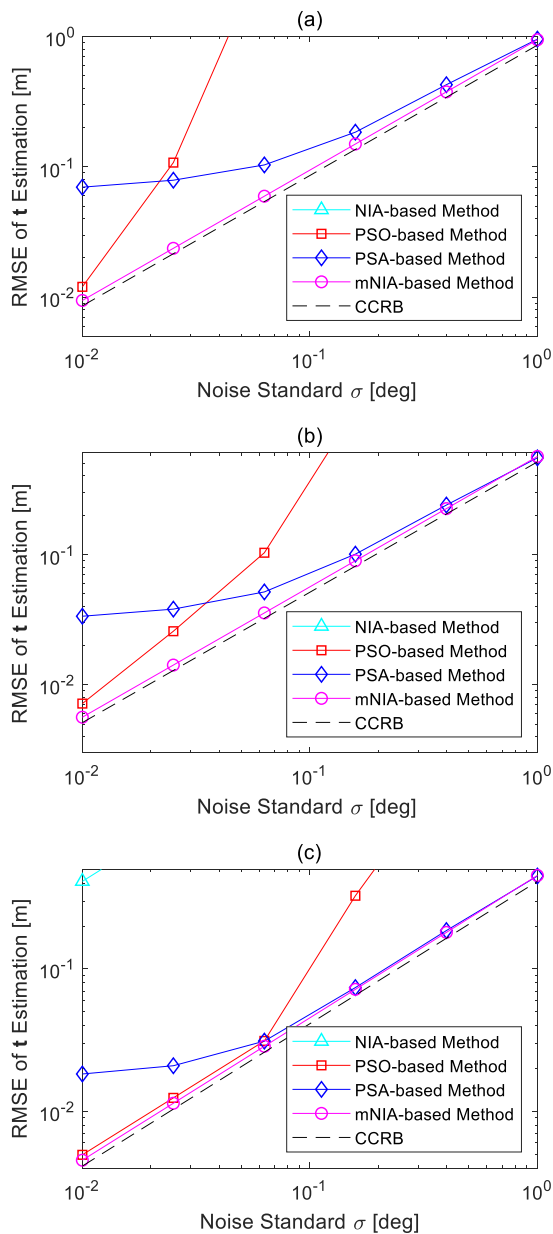**FIGURE 5.** Estimation RMSE comparison of the four methods in terms of the rotation matrix R of targets in different sizes (a) *D* = 1 meter, (b) *D* = 2 meters, (c) *D* = 3 meters.

FIGURE 6. Estimation RMSE comparison of the four methods in terms of the translation vector t of targets in different sizes (a) *D* = 1 meter, (b) *D* = 2 meters, (c) *D* = 3 meters.

where $\hat{\mathbf{R}}_n$ and $\hat{\mathbf{t}}_n$ mean the estimates in the nth Monte Carlo iteration. The RMSEs of the translation vector (location) and the rotation matrix (attitude) are respectively shown in Figures 5 and 6 under different levels of noise and different target sizes.

The CCRBs [19] of the estimates of $\mathbf{R}$ and $\mathbf{t}$ in the AoA-based RBL scheme is also given as reference. It is widely known that, CCRB can give a lower bound for the estimating variance of the parameter estimation problems with constraints, and CCRB is widely applied for the field of localization. For providing a benchmark of the estimation performance over a small noise region (derivation of the
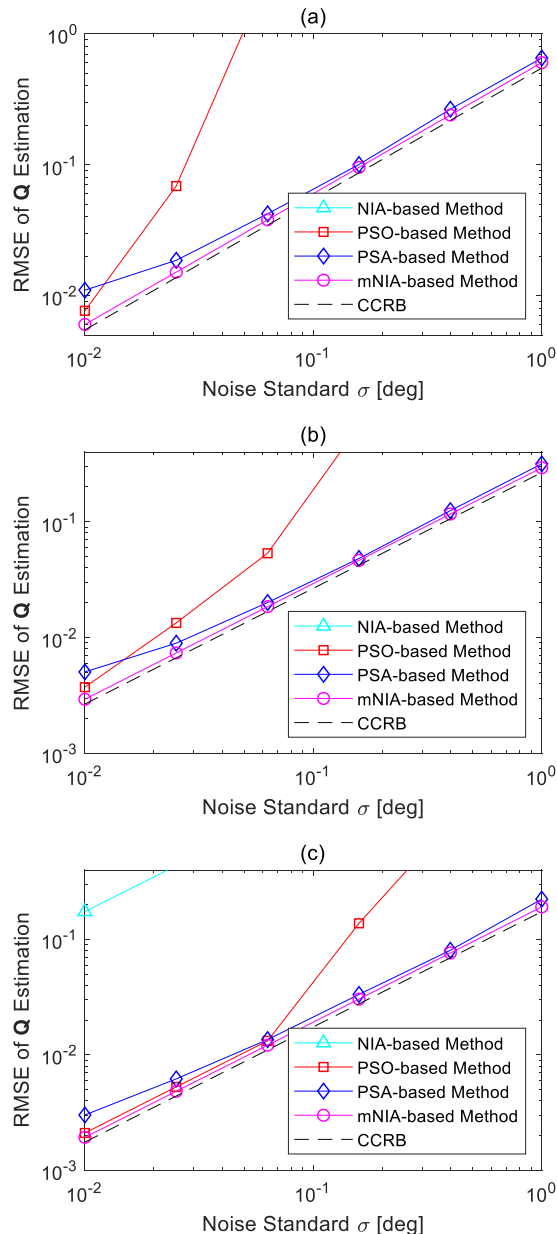
CCRB for the considered RBL framework is presented in Appendix).

Here we should note is that currently existing RBL models mainly focusing on utilizing ranging-based measurements, e.g. TDoA and ToA, for information fusing. Hence, it is unfeasible to add ranging-based approaches for comparison because that the parameters affecting the RBL performance are different. In ranging-based schemes, the effecting parameters include the number of BSs and the synchronization error, etc.; while in the AoA-based RBL scheme adopting only a single BS, the AoA measurement accuracy and the size of the rigid body need to be considered. Besides, the

superiority of AoA-based RBL model over the ranging based RBL model has be discussed in detail in the Section II.A. Hence, for comparison, we simulated the RBL schemes using the traditional NIA method [25], and the PSO algorithm [19] and the PSA method [20] and provide CCRB as a criterion for these methods.

As it can be seen from the figures, the AoA-based RBL scheme via a single BS has a remarkable accuracy: when the rigid target is 8 meters away from the single BS and when the AoA measuring noise is around 0.1 deg, the positioning error can reach to the centimeter level and the attitude estimation is also impressive, when the AoA measuring noise is around 0.1 deg. According to the results shown in Figures 5 and 6, the RMSEs of estimates decrease as the noise level of AoA reduces as we expected. Moreover, larger size of rigid target can improve the CSR and RMSE of the RBL performance. With a larger D, the differences of AoA between wirless sensors increases, by which the bigger D can avoid the AoA measuring interference, which enhances RBL robustness against AoA estimation noise. This conclusion indicates that reasonable sensor distribution is that the sensor should be fixed on the target as far apart as possible.

It is observed that the proposed mNIA-based RBL scheme is closest to the CCRB, which verifies its superiority over the other three methods. The RBL performance of the traditional NIA-based method is also shown in the figures; however, because of its low convergence success rate results in huge RBL error, we even barely see its performance in the comparison range. Theoretically speaking, the performance gap between the mNIA-based method and the NIA-based method is zero, if there is no convergence failure. Similarly, the estimation RMSE of the PSO-based method is also beyond the comparison range at a higher level of noise, due to the low convergence success rate. But at the lower noise level, the PSO method outperforms the PSA method when there is no convergence failure, while the PSA-based method performs better at higher noise level.

VI. CONCLUSION AND FUTURE WORK
In this paper, the RBL framework based on the AoA measurement was considered for the Internet of Things (IoT) applications, in which a single BS is used to estimate the position and attitude of the rigid body target. Several wireless sensor nodes were fixed on the rigid object and their pairwise distances are foreknown; meanwhile, the AoA of the wireless signals from the nodes to the single BS was measured. By merging the topology information with the AoA measurements, we could obtain the 3-D coordinates of each node. For the information fusion, we proposed the modified Newton's iteration algorithm, considering the range information of the RBL scenario and the information vector fitness. Then position and attitude information of rigid target relative to the reference frame was determined by UQ method. Finally, the performance of the proposed method was evaluated by simulations. The simulation results indicate that comparing with the heuristic algorithms and the traditional Newton's iteration algorithm,

the proposed RBL method shows its superiority of fast speed and high success rate, and finer RBL performance approximating the CCRB.

During the simulations, it is indicated that the size of the target has an important impact on the convergence success rate and the RMSE performance. Actually, it is the topology information that matters to the RBL performance. Hence, the influence from the deployment of wireless nodes, including the topology information and the adopted sensor number, should be explored; in addition, the uncertainty of the topology information is another worthwhile topic for testing the robustness of the AoA-based RBL framework adopting a single BS in the smart sensing network. The above two issues will be investigated in our future works.

APPENDIX
CCRB DERIVATION FOR AOA-BASED RBL FRAMEWORK
In the considered RBL framework, the parameters to be estimated consist of the translation vector $\mathbf{t} = [x, y, z]^T$ and the rotation matrix $\mathbf{R} = [\mathbf{r}_1 \ \mathbf{r}_2 \ \mathbf{r}_3]$. We collect the parameters using a 12×1 composite vector $\boldsymbol{\rho} = [\mathbf{r}_1^T, \ \mathbf{r}_2^T, \ \mathbf{r}_3^T, \ \mathbf{t}^T]^T$. Because $\mathbf{R}^T\mathbf{R} = \mathbf{R}\mathbf{R}^T = \mathbf{I}_3$, the unknown vector $\boldsymbol{\rho}$ is then subject to equality constraints and The CCRB of $\boldsymbol{\rho}$ has form [31]

$$CCRB\left(\boldsymbol{\rho}\right) \geq \mathbf{M}\left(\mathbf{M}^T\mathbf{F}(\boldsymbol{\rho})\mathbf{M}\right)^{-1}\mathbf{M}^T, \qquad (28)$$

where $\mathbf{M} \in \mathbb{R}^{12 \times P}$ is decided by the equality constraint as follows

$$\mathbf{M} = \begin{bmatrix} -\mathbf{r}_3 & \mathbf{0}_{3\times 1} & \mathbf{r}_2 & \\ \mathbf{0}_{3\times 1} & -\mathbf{r}_3 & -\mathbf{r}_1 & \mathbf{0}_{9\times 3} \\ \mathbf{r}_1 & \mathbf{r}_2 & \mathbf{r}_{3\times 1} & \\ & \mathbf{0}_{3\times 3} & & \sqrt{2}\cdot\mathbf{I}_3 \end{bmatrix}; \qquad (29)$$

and $\mathbf{F}(\boldsymbol{\rho})$ is the Fisher information matrix (FIM) resulted by $\mathbf{F}\left(\boldsymbol{\rho}\right) = -E\left[\frac{\partial^2 \ln p(\boldsymbol{\alpha},\boldsymbol{\beta};\boldsymbol{\rho})}{\partial\boldsymbol{\rho}\boldsymbol{\rho}^T}\right]$, in which $p\left(\boldsymbol{\alpha}, \boldsymbol{\beta}; \boldsymbol{\rho}\right)$ is the likelihood of $\boldsymbol{\alpha}$ and $\boldsymbol{\beta}$; since we assume AoA measurements follow the independent Gaussian distribution, $p\left(\boldsymbol{\alpha}, \boldsymbol{\beta}; \boldsymbol{\rho}\right)$ equals

$$p\left(\boldsymbol{\alpha}, \boldsymbol{\beta}; \boldsymbol{\rho}\right) = \frac{1}{\left(2\pi\sigma^2\right)^{\frac{K}{2}}} * \exp\left\{-\left[\frac{1}{2\sigma^2} * \sum_{k=1}^{K}\left(\left(\alpha_k - \alpha_k^o\right)^2\right.\right.\right.$$
$$\left.\left.\left. + \left(\beta_k - \beta_k^o\right)^2\right)\right]\right\}. \quad (30)$$

REFERENCES
[1] X. Huang, W. Guo, G. Liu, and G. Chen, "FH-OAOS: A fast four-step heuristic for obstacle-avoiding octilinear Steiner tree construction," *ACM Trans. Des. Autom. Electron. Syst.*, vol. 21, no. 3, 2016, Art. no. 48.

[2] P. J. From, "Rigid body dynamics," in *Vehicle-Manipulator Systems*. London, U.K.: Springer, 2014, pp. 191–227.

[3] R. Featherstone, *Robot Dynamics Algorithms*. Norwell, MA, USA: Kluwer, 1987.

[4] C. Di Natali, M. Beccani, N. Simaan, and P. Valdastri, "Jacobian-based iterative method for magnetic localization in robotic capsule endoscopy," *IEEE Trans. Robot.*, vol. 32, no. 2, pp. 327–338, Apr. 2016.

[5] A. I. Mourikis, N. Trawny, S. I. Roumeliotis, A. E. Johnson, A. Ansar, and L. Matthies, "Vision-aided inertial navigation for spacecraft entry, descent, and landing," *IEEE Trans. Robot.*, vol. 25, no. 2, pp. 264–280, Apr. 2009.

[6] H. Y. Xu, Y. Zhang, B. Ba, D. Wang, and X. Li, "Fast joint estimation of time of arrival and angle of arrival in complex multipath environment using OFDM," *IEEE Access*, vol. 6, pp. 60613–60621, 2018.

[7] M. Pedley, "Tilt sensing using a three-axis accelerometer," Freescale Semicond., Appl. Note AN3461, Feb. 2012.

[8] C. Forster, L. Carlone, F. Dellaert, and D. Scaramuzza, "IMU preintegration on manifold for efficient visual-inertial maximum-a-posteriori estimation," *Proc. Robot., Sci. Syst.*, 2015. [Online]. Available: https://smartech.gatech.edu/handle/1853/55417

[9] J.-C. Juang and G.-S. Huang, "Development of GPS-based attitude determination algorithms," *IEEE Trans. Aerosp. Electron. Syst.*, vol. 33, no. 3, pp. 968–976, Jul. 1997.

[10] M. J. Bentum, C. J. M. Verhoeven, A. J. Boonstra, E. K. A. Gill, and A. J. van der Veen, "A novel astronomical application for formation flying small satellites," in *Proc. 60th Int. Astron. Congr.*, Daejeon, South Korea, Oct. 2009, pp. 1–8.

[11] S. P. Chepuri, G. Leus, and A.-J. van der Veen, "Rigid body localization using sensor networks," *IEEE Trans. Signal Process.*, vol. 62, no. 18, pp. 4911–4924, Sep. 2014.

[12] S. Chen and K. C. Ho, "Accurate localization of a rigid body using multiple sensors and landmarks," *IEEE Trans. Signal Process.*, vol. 63, no. 24, pp. 6459–6472, Dec. 2015.

[13] J. Jiang, G. Wang, and K. C. Ho, "Accurate rigid body localization via semidefinite relaxation using range measurements," *IEEE Signal Process. Lett.*, vol. 25, no. 3, pp. 378–382, Mar. 2018.

[14] J. Jiang, G. Wang, and K. C. Ho, "Sensor network-based rigid body localization via semi-definite relaxation using arrival time and Doppler measurements," *IEEE Trans. Wireless Commun.*, vol. 18, no. 2, pp. 1011–1025, Feb. 2019.

[15] B. Hao, K. C. Ho, and Z. Li, "Range based rigid body localization with a calibration emitter for mitigating anchor position uncertainties," *IEEE Trans. Wireless Commun.*, to be published.

[16] A. M. Toufik, J. Yao, and Y. Jin, "Chorus-line algorithm for clock synchronization," *IEEE Access*, vol. 6, pp. 8412–8425, 2018.

[17] A. Pizzo, S. P. Chepuri, and G. Leus, "Towards multi-rigid body localization," in *Proc. IEEE Int. Conf. Acoust., Speech Signal Process. (ICASSP)*, Shanghai, China, Mar. 2016, pp. 3166–3170.

[18] B. Li, W. Bai, and G. Zheng, "Successive ESPRIT algorithm for joint DOA-range-polarization estimation with polarization sensitive FDA-MIMO radar," *IEEE Access*, vol. 6, pp. 36376–36382, 2018.

[19] B. Zhou, L. Ai, X. Dong, and L. Yang, "DoA-based rigid body localization adopting single base station," *IEEE Commun. Lett.*, vol. 23, no. 3, pp. 494–497, Mar. 2019.

[20] B. Zhou, X. Yao, L. Yang, S. Yang, S. Wu, Y. Kim, and L. Ai, "Accurate rigid body localization using DoA measurements from a single base station," *Electronics*, vol. 8, no. 6, p. 622, 2019.

[21] X. Huang, G. Liu, W. Guo, Y. Niu, and G. Chen, "Obstacle-avoiding algorithm in X-architecture based on discrete particle swarm optimization for VLSI design," *ACM Trans. Des. Autom. Electron. Syst.*, vol. 20, no. 2, 2015, Art. no. 24.

[22] B. Lin, W. Guo, and X. Lin, "Online optimization scheduling for scientific workflows with deadline constraint on hybrid clouds," *Concurrency Comput., Pract. Exper.*, vol. 28, no. 11, pp. 3079–3095, 2016.

[23] Y. Cheng, H. Jiang, F. Wang, Y. Hua, D. Feng, W. Guo, and Y. Wu, "Using high-bandwidth networks efficiently for fast graph computation," *IEEE Trans. Parallel Distrib. Syst.*, vol. 30, no. 5, pp. 1170–1183, Mar. 2019.

[24] Y. Sun and Q. Wan, "Position determination for moving transmitter using single station," *IEEE Access*, vol. 6, pp. 61103–61116, 2018.

[25] K. Zhou, X. Wang, Z. Wang, H. Wei, and L. Yin, "Complete initial solutions for iterative pose estimation from planar objects," *IEEE Access*, vol. 6, pp. 22257–22266, 2018.

[26] H. Jamali-Rad and G. Leus, "Dynamic multidimensional scaling for low-complexity mobile network tracking," *IEEE Trans. Signal Process.*, vol. 60, no. 8, pp. 4485–4491, Aug. 2012.

[27] Z. X. Chen, H. W. Wei, Q. Wan, S. F. Ye, and W. L. Yang, "A supplement to multidimensional scaling framework for mobile location: A unified view," *IEEE Trans. Signal Process.*, vol. 57, no. 5, pp. 2030–2034, May 2009.

[28] B. Zhou, C. Jing, and Y. Kim, "Joint TOA/AOA positioning scheme with IP-OFDM systems," *Wireless Pers. Commun.*, vol. 75, no. 1, pp. 261–271, 2014.

[29] J. Diebel, "Representing attitude: Euler angles, unit quaternions, and rotation vectors," *Matrix*, vol. 58, nos. 15–16, pp. 1–35, 2006.

[30] Z. Teng, "Surface-based 3D object modeling, detection, and pose estimation in cluttered environments for robotic manipulation," Ph.D. dissertation, College Comput. Inform., Univ. North Carolina Charlotte, Charlotte, NC, USA, 2016.

[31] E. Nitzan, T. Routtenberg, and J. Tabrikian, "Cramér–Rao bound for constrained parameter estimation using Lehmann-unbiasedness," *IEEE Trans. Signal Process.*, vol. 67, no. 3, pp. 753–768, Feb. 2019.

[32] Z. Shen, P. P. C. Lee, J. Shu, and W. Guo, "Encoding-aware data placement for efficient degraded reads in XOR-coded storage systems: Algorithms and evaluation," *IEEE Trans. Parallel Distrib. Syst.*, vol. 29, no. 12, pp. 2757–2770, Dec. 2018.

[33] X. Li and W. Zhu, "Two-stage layout decomposition for hybrid E-beam and triple patterning lithography," *ACM Trans. Des. Autom. Electron. Syst.*, vol. 23, no. 1, 2017, Art. no. 6.

[34] H. Cheng, N. Xiong, L. T. Yang, and Y-S. Jeong, "Distributed scheduling algorithms for channel access in TDMA wireless mesh networks," *J. Supercomput.*, vol. 63, no. 2, pp. 407–430, 2013.

[35] W. Zhu, J. Chen, and W. Li, "An augmented Lagrangian method for VLSI global placement," *J. Supercomput.*, vol. 69, no. 2, pp. 714–738, 2014.

[36] X. Zheng, X. Zhang, Y. Yu, T. Kechadi, and C. Rong, "ELM-based spammer detection in social networks," *J. Supercomput.*, vol. 72, no. 8, pp. 2991–3005, 2016.

[37] X. Zheng, D. An, X. Chen, and W. Guo, "Interest prediction in social networks based on Markov chain modeling on clustered users," *Concurrency Comput., Pract. Exper.*, vol. 28, no. 14, pp. 3895–3909, 2016.

[38] J. Chen, Y. Liu, Z. Zhu, and W. Zhu, "An adaptive hybrid memetic algorithm for thermal-aware non-slicing VLSI floorplanning," *Integration*, vol. 58, pp. 245–252, Jun. 2017.

[39] Y. Yang, X. Zheng, V. Chang, and C. Tang, "Semantic keyword searchable proxy re-encryption for postquantum secure cloud storage," *Concurrency Comput., Pract. Exper.*, vol. 29, no. 19, 2017, Art. no. e4211.
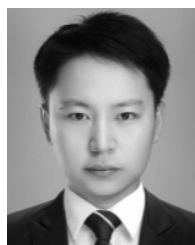
BIAO ZHOU (M'18) received the B.S. degree from the Qingdao University of Science and Technology, China, in 2011, and the Ph.D. degree from Kwangwoon University, Seoul, South Korea, in 2016. He is currently working as an Assistant Professor with the School of the Internet of Things Engineering, Jiangnan University, Wuxi, China. His research interests include passive tracking and localization systems in wireless sensor networks, including positioning model building, and optimization.

MINGMING ZHANG is currently pursuing the master's degree in arts and design with the School of Digital Median, Jiangnan University, Wixi, China. Her research interests on inclusive digital arts, new media exhibition, virtual reality, digital scene design, and behavior analysis.

YU-QIANG CHEN received the Ph.D. degree from the Guangdong University of Technology. He is currently a Professor with the Department of Computer Engineering, Dongguan Polytechnic, China. His current research interests include network security, the mobile internet, big data, the IoT, and cryptography.

NAIXUE XIONG received the Ph.D. degrees from Wuhan University and the Japan Advanced Institute of Science and Technology. He worked with Northeastern State University, Georgia State University, Wentworth Technology Institution, and Colorado Technical University (a Full Professor about five years) about ten years. He is currently a Professor with the College of Intelligence and Computing, Tianjin University, China.

YUAN TIAN received the master's and Ph.D. degrees from Kyung Hee University. She is currently working as an Assistant Professor with the College of Computer and Information Sciences, King Saud University, Saudi Arabia. She is also working as a Research Fellow with the School of Computer Engineering, Nanjing Institute of Technology. Her research interests are broadly divided into privacy and security, which are related to cloud computing, bioinformatics, multimedia, cryptograph, smart environment, and big data.

SABBIR AHMED is currently pursuing the M.S. degree with the IoT Engineering Research Center, Ministry of Education, Jiangnan University, China. His research interests include the intelligent recognition algorithms and the signal processing.

● ● ●